Adaptive brain changes to virtual lesions interfering with visual processing

Short title: BOLD correlates of virtual lesions in the visual system

Estelle RAFFIN[1,2], Roberto F. SALAMANCA-GIRON[1,2], Krystel R. HUXLIN[3], Olivier REYNAUD[4], Loan MATTERA[4], Roberto MARTUZZI[4], Friedhelm C. HUMMEL[1,2,5]

[1] Defitech Chair of Clinical Neuroengineering, Neuro-X Institute (INX) and Brain Mind Institute (BMI), Ecole Polytechnique Fédérale de Lausanne (EPFL), Geneva, Switzerland.

[2] Defitech Chair for Clinical Neuroengineering, INX and BMI, EPFL Valais, Clinique Romande de Réadaptation, Sion, Switzerland.

[3] The Flaum Eye Institute and Center for Visual Science, University of Rochester, Rochester, NY, USA.

[4] Human Neuroscience Platform, Fondation Campus Biotech Genève (FCBG), Campus Biotech, Geneva, Switzerland.

[5] Department of Clinical Neurosciences, Geneva University Hospital (HUG), Geneva, Switzerland.

Corresponding Author: Estelle Raffin, Defitech Chair of Clinical Neuroengineering, Neuro-X Institute (INX) and Brain Mind Institute (BMI), Ecole Polytechnique Fédérale de Lausanne (EPFL) - Campus Biotech, Room H4.3.132.084, Chemin des Mines 9, 1202 Geneva, Switzerland., Email: estelle.raffin@epfl.ch.

Highlights:

- TMS-induced perturbation of the early visual areas (EVA) or the mediotemporal area (hMT+/V5) area selectively impairs motion direction discrimination.
- The TMS perturbation is associated with a local down-scaling of BOLD activity in both areas, potentially specific to task-related neuronal populations during motion discrimination.
- The two visual areas display distinct topological networks' adaptations in response to TMS, reflecting different levels of networks resilience to a focal lesion.
- TMS-fMRI coupling can be used to assess 'disconnectomics' and to precisely map how a local perturbation propagates to large-scale behavioural deficits.

38 **Graphical abstract**

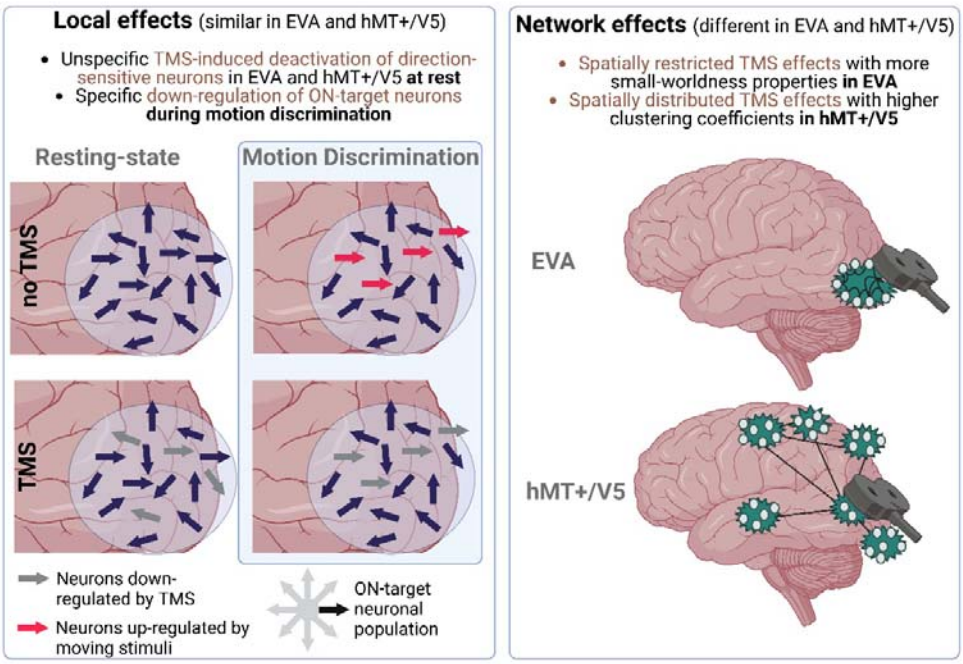

39

Abstract:

Understanding the causal relationship between a focal lesion and network (re)organization is crucial to accurately predict the resulting large-scale symptoms of a lesion. In this study, we applied short trains of 10 Hz TMS to healthy participants over the early visual areas (EVA) or the medio-temporal area (hMT+/MT) during a motion discrimination task and at rest, while concurrent fMRI was acquired. TMS applied in the early stage of motion processing induced a specific deficit in judging motion direction in both sites, while global motion perception was preserved. This was associated with a common suppression of local brain activity and network activity. In contrast, we report distinct topological network properties depending on the disrupted site. Networks associated with EVA perturbation displayed a more robust and efficient functional reorganization, suggesting that EVA might be more resilient to focal perturbations. While contributing to a better understanding of the impact and potential mechanisms of TMS perturbation, these results provide a model for focal lesions in the visual motion processing system.

1. Introduction:

Brain networks dynamically adjust their spatiotemporal organization to changing contexts and ongoing demands (Telesford et al., 2011) (Papo et al., 2014). Such adaptive networks can be characterized by their topological transformation, their state-dependency and/or their state transition. The adaptive nature of brain networks is likely important for maintaining an optimal balance of information segregation and integration, allowing functional stability, communication via long-range connections, all while maximizing the efficiency of local processing. This process might support functional networks resilience in case of progressive neurodegeneration or focal lesions (Bullmore and Sporns, 2012) (Bassett and Bullmore, 2009) (Fornito et al., 2015). Today, a comprehensive understanding of the causal relationship between a focal lesion and brain network organization is still missing despite the fact that lesion-based brain disorders are network disorders, leading to the inability to accurately predict resulting symptoms and recovery processes.

Directly testing the systematic association between a focal lesion and brain reorganization in humans is challenging, because of the difficulties inherent in selectively altering activity *in vivo* to dissect causal impact on brain networks. An emerging approach is to combine non-invasive brain stimulation (e.g., transcranial magnetic stimulation, TMS) with neuroimaging techniques (in particular functional magnetic resonance imaging (fMRI)) (Ozdemir et al., 2020) (Vink et al., 2018) (Bergmann et al., 2021). The combination of TMS with fMRI provides a unique opportunity to temporarily "knock out" a brain region and assess the changes in local brain activity and inter-areal functional connectivity that may underlie changes in task performance (Ruff et al., 2006) (Bestmann S., 2008) (Ricci et al., 2012) (Leitão et al., 2015) (Cocchi et al., 2016) (Beckers and Hömberg, 1992). The first use of the so-called "TMS-induced virtual

lesion" concept was in early visual cortex, to impair visual targets' detection (Amassian et al., 1989). Later, several attempts have been made to combine fMRI with TMS to capture the impact that TMS can have on patterns of functional connectivity in specialized, large-scale, brain systems (Ruff et al., 2008) (Jung et al., 2020). However, the nature and functional relevance of the local brain responses to TMS induced virtual lesions and network changes are still unclear. This lack of knowledge prevents the use of TMS perturbation as a proper model to precisely map how a local perturbation propagates to large scale behavioural deficits and establish it as a model for lesion-based neurological disorders.

Whether single pulse TMS actually modulates local BOLD activity is currently debated in the field (Rafiei and Rahnev, 2022). In the context of virtual lesions or TMS perturbations, diverging hypotheses have been suggested. Virtual lesions are classically associated with a temporary inactivation of a population of neurons (Ruzzoli et al., 2010) (Perini et al., 2012) (Schwarzkopf et al., 2011) (Wahlbom et al., 2019). Prior studies using concurrent or interleaved TMS and fMRI have described a localized decreased BOLD signal as being the neural signature of TMS-induced virtual lesions (Sack et al., 2007) (Ruff et al., 2008) (Harris et al., 2008) (Mullin and Steeves, 2013) (Mason et al., 2014). In contrast, proponents of the *random noise activity* hypothesis state that TMS actually acts by inducing random neuronal activity that is unrelated to the ongoing activity (Pascual-Leone et al., 1999) (Silvanto and Muggleton, 2008) (Ruzzoli et al., 2010) (Schwarzkopf et al., 2011) (Solomon-Harris et al., 2016), suggesting that TMS preferentially recruits populations of neurons that are not involved in the on-going cognitive process. This theory received support from behavioral and modeling studies (Bancroft et al., 2014), but so far no neuroimaging data have reported correlates of this TMS-induced random noise activity. Prior literature on online homeostatic regulation of brain activity (Billman, 2020), would rather suggest that TMS preferentially acts on the

110 neural populations that are pre-activated by a task for instance, hereby achieving higher
111 functional selectivity of targeted populations. Here we hypothesized that pre-activating
112 a given population of neurons locally through a behavioural task would make them more
113 sensitive to TMS effects.

114 Beside local effects, substantial evidence have shown that TMS can modulate
115 connected remote brain areas (Bestmann et al., 2004) (Denslow et al., 2005) (Solomon-
116 Harris et al., 2016) (Tik et al., 2017) (Jung et al., 2020). It is also very likely that signal
117 propagation, interareal interactions are context dependent and shaped by the
118 hierarchical level of the brain area that is targeted. In an elegant modelling study, Gollo
119 and collaborators compared the impact of an inhibitory rTMS protocol when applied to
120 a brain hub region or to a peripheral region (Gollo et al., 2017). Their results revealed
121 that brain hubs, where activity is integrated and further distributed appear to be
122 functionally less affected by focal perturbations. In contrast, perturbations of peripheral
123 and more associative areas, might have greater impact on acute network activity. To test
124 it in vivo, we compared the level of network activity in different behavioural contexts
125 and the topological features of brain networks in response to a virtual lesion of the early
126 visual areas (EVA) and of the extrastriate, motion-sensitive visual area hMT+/V5. These
127 two regions were chosen because they allowed us to compare the whole brain
128 consequences of a virtual lesion affecting a primary integrative brain region, acting as a
129 gateway to other 'higher' visual areas, and in contrast, a more functionally specialized
130 brain region (Grossberg et al., 1999; Mineault et al., 2012; Rust et al., 2006; Simoncelli
131 and Heeger, 1998). Hierarchical models have been used to explain motion processing in
132 the dorsal stream of the visual cortex (Giese and Poggio, 2003; Grossberg et al., 1999;
133 Mineault et al., 2012; Rust et al., 2006; Simoncelli and Heeger, 1998). Most of these
134 models assume that V1 measures motion inaccurately while hMT+/V5 performs certain
135 calculations on the V1 output to obtain the correct direction and speed (Pack and Born,

136 2010). Hence, hMT+/V5 is thought to belong to a second order region, which conversely
137 to V1, only receives specialized motion signals (see also (Zhang and Tadin, 2019)). We
138 applied ICA and graph analyses to provide a qualitative and quantitative framework and
139 compared whole brain functional networks under different conditions of TMS induced
140 perturbation. We anticipated that the degree of distributed networks underlying TMS
141 effects would explain differences in robustness to EVA or to hMT+/V5 disruption (Das et
142 al., 2012) (Gollo et al., 2017) (Tu et al., 2021). More precisely, we hypothesized that EVA,
143 as a primary integrative brain region, would show a more robust network organization in
144 response to TMS, as measured with network topology metrics, namely higher degrees of
145 small-world networks with shorter characteristic path length and larger clustering
146 compared to hMT+/V5.

147 In sum, we compared the behavioural consequences, as well as the local and network
148 activation associated with TMS-induced perturbation applied to the EVA or to hMT+/V5
149 at rest and during a motion direction discrimination task with different TMS timings. We
150 expected TMS perturbations to selectively alter neuronal populations involved in the
151 task for both stimulated regions in proportion with behavioral impairments. If our
152 expectations are verified, we would provide neuroimaging evidence supporting the use
153 of active tasks to improve selectivity of TMS effects (Romero et al., 2019). Furthermore,
154 we anticipated that signal propagation would differ depending on the hierarchical
155 network level of the stimulated area, providing an *in vivo* model to study differences in
156 the resulting large-scale behavioral deficits of a focal brain lesion depending on lesion
157 site.

158

159 ## 2. Methods

160

161 ***Participants***

162 In total, thirty healthy subjects (seventeen males: mean age 28.8 years, range 19–39
163 years) were recruited in the experiment. All participants provided informed written
164 consent prior the experiment and none of them met the MRI or TMS exclusion criteria
165 (Rossi et al., 2021). This study was approved by the local Swiss Ethics Committee (2017-
166 01761) and performed in accordance with the Declaration of Helsinki.

167

168 ***Experimental Design and Task Procedure***

169 Sixteen participants (nine males, mean age 26.5 years, range 19-32 years) performed
170 two TMS-fMRI sessions (except one drop-out for the second session). During the first
171 session, TMS was applied to the right EVA ($TMS_{(EVA)}$: mean(±SD) MNI coordinate: 8(5);-
172 76(4);9(6)) using phosphenes perception when possible (in 9/16 participants) or the O2
173 position based on the 10-20 EEG system; during the second session, TMS was applied to
174 the functionally defined right hMT+/V5 ($TMS_{(hMT+/V5)}$: mean MNI coordinates (SD): 46(4);
175 -83(6); 11(5)) (Figure 1A). We chose this study design to maximize our chances to
176 optimally target the individual hMT+/V5 area through a dedicated MT localizer acquired
177 during the first session (see online supplementary materials for a description of the
178 hMT+/V5 functional localizer). For the two online TMS-fMRI sessions, TMS was applied
179 during a *motion direction discrimination (MDD) Task* and at *Rest*. These sessions had the
180 same content except the anatomical T1-MPRAGE sequence and the hMT+/V5 functional
181 localizer sequence, which were only performed during the first session. A short offline
182 session prior the hMT+/V5 session was needed to locate the individual hMT+/V5 cluster
183 using a neuro-navigation system (Localite GmbH, Bonn, Germany).

184 An offline control experiment was performed to control for TMS non-specific effects on
185 additional fifteen participants (seven males, mean age 28.9 years, range 22-39 years).
186 We repeated the *MDD task* with TMS using the same setup (neuronavigation and eye-

tracking systems) and the same task parameters (see below) but stimulating the right motor cortex ($TMS_{(M1)}$, mean(SD) MNI coordinates: 53(7);-4(2);54(3), corresponding to the motor hotspots of the participants), outside the MRI scanner. Figure 1B summarizes the study timeline.

For the three sessions, the *MDD task* consisted in rating subjective perceptual experience of visually presented motion stimuli and in performing a forced-choice direction discrimination task on the same moving stimuli (Koivisto et al., 2021). The visual stimuli involved a group of static or moving dots coherently to the right or to the left. During the familiarization phase outside the scanner, the duration of stimulus presentation was individually defined (either 50, 67 or 84 ms, corresponding to 3, 4 or 5 frames) to ensure approximatively 70% accuracy in the *noTMS* trials. The stimulus duration was then kept constant throughout the experiment (see Figure 1D for an illustration of the task).

Just after the stimulus presentation, participants were asked to rate their perception using a response box with their right hand using a 1 to 4 scale (see Figure 1's caption for more details). In the main experimental conditions, TMS bursts were given to EVA when visual signals first reach the target region 60 ms after the onset of the visual stimulus ($TMS_{(EVA)}$) (Lamme, 2001) and 30 ms after stimulus onset ($TMS_{(hMT+/V5)}$) for hMT+/V5 to account for the direct thalamic-extrastriate pathway (Lamme and Roelfsema, 2000) (Beckers and Homberg, 1992) (d'Alfonso et al., 2002) (Koivisto et al., 2010). This ensured similar perturbation of the feed-forward thalamic inputs to the two regions. Later TMS onsets were also tested in half of the trials, 100ms for EVA and 130ms for hMT+/V5 selectively interfering with late processing stages. The total direction of the TMS bursts was 200ms to cover the full window of visual processing in the two regions. TMS intensity was set to ≈ 80% [range: 75 to 90%] maximal stimulator output (MSO) for the

212 *HighTMS* condition. Intensity was individually adjusted prior the measurement to ensure
213 phosphene sub-threshold stimulation and progressively increased until participants
214 report pain or discomfort. The intensity was then chosen to get reliable BOLD signal
215 while preserving participant's comfort. For the M1 control experiment, the same EVA
216 timings were used and TMS was given sub-threshold to avoid motor evoked potentials
217 elicitation.

218 Conditions randomly alternated between TMS versus noTMS trials, moving versus static
219 trials throughout the task, 50 trials each, giving a total of 300 trials. An inter-trial interval
220 (ITI) of approximatively 1.5 sec was used. The task was displayed in the scanner through
221 a 44cm x 27cm LCD monitor at a 2.5m distance via a mirror mounted on the head coil,
222 on a frame on top of the TMS-fMRI setup (Figure 1B). For the offline M1 control
223 experiment, the task was displayed on a mid-grey background LCD projector (1024 x
224 768, 144 Hz). To exclude bad performance due to TMS-induced blinking and to make
225 sure that participants were constantly looking at the fixation point, gaze and pupils'
226 movements were controlled in real time with an EyeLink 1000 Plus Eye Tracking System
227 (SR Research Ltd., Canada) in the scanner and in the behavioral room, sampling at a
228 frequency of 1000 Hz. Trials were aborted and redone if deviation exceeded 1° from the
229 fixation point. The duration of the *MDD Task-TMS* sequence was on average 16.5
230 minutes (SD = 4.30 minutes) depending on individual reaction times.

231 - A *Rest-TMS* sequence, during which an event-related design was used to map the
232 effect of TMS bursts composed of three pulses at alpha (10Hz) frequency. Three
233 conditions were pseudorandomized and counterbalanced across the run: high-intensity
234 TMS (*HighTMS)*, low-intensity TMS *(LowTMS)* and no TMS *(noTMS),* with 25 repetitions
235 of each condition with an inter-trial interval (ITI) of 6 seconds (covering 3 repetition
236 times). *HighTMS* intensity corresponded to the intensity used during the MDD Task

while *LowTMS* was set to ≈38 % [35 to 43%] MSO. Participants were asked to look at a fixation cross throughout the acquisition. Note that the LowTMS data are not reported in this manuscript. The duration of the *Rest TMS* sequence was 9 minutes.

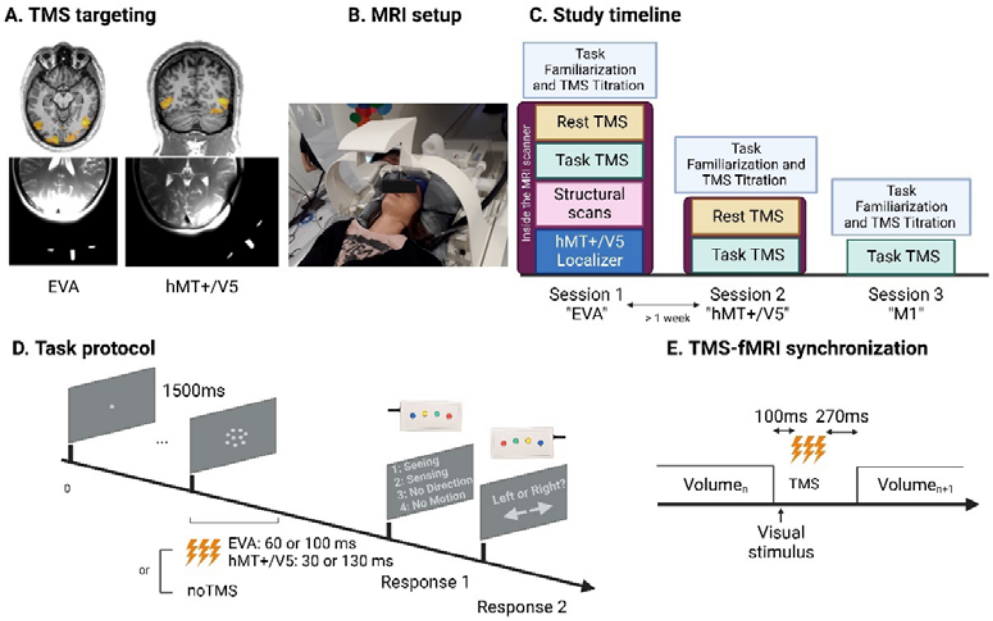

Figure 1.A: TMS targeting*. TMS targets were determined by the functional localizer of EVA and hMT+/V5 for precise TMS positioning (see online materials for further details about the motion processing localizer). The two images on the right part show the T2 image of a representative subject with the oil capsules placed on the TMS-MRI coil casing to monitor the coil position located on the TMS coil for V1 and V5. These markers formed a "T-like shape" indicating the center of the coil as well as the coil orientation as seen on a T2 HASTE image acquired with the two TMS-compatible MRI coil arrays (56 axial slices, slice thickness = 0.8 mm, TR = 1500 ms, TE = 135 ms, FOV = 216 mm, flip angle = 140°).* Coil positions were readjusted if needed. ***B: MRI setup****. The MRI-TMS coil was positioned over the occipital area while the MR-receiving coil was positioned over the frontal lobe. Both were maintained via a vacuum pillow to ensure the absence of movement or vibration and to ensure a comfortable position for the participant.* ***C: Study timeline****: Description of the two experimental sessions;* ***D: One single trial of the motion discrimination task****. The visual stimuli involved a group of white dots in a 5˚ diameter circular aperture centered in the middle of the screen. The dots were either static or moving coherently to the right or to the left at a density of 2.6 dots per degree. Dots were displayed for 50, 67 or 84 ms (corresponding to 3, 4 or 5 frames). This duration was individually adjusted prior the fMRI measurement to ensure approximatively 70% accuracy in the noTMS trials.* Just after the stimulus presentation, participants were asked to subjectively rate their perception using a response box on their right hand with a 1 to 4 scale, 1 being "I clearly saw the motion" (Seeing), 2 being "I sensed the motion" (Sensing), 3 being "I saw something moving but I'm unable to judge the direction" (No Direction) and 4 being "I didn't see any motion" (No Motion) (Koivisto et al., 2010) (Grasso et al., 2018). When the participants pressed the three first options, they were then asked to judge whether the dots moved to the right or to the left with a response box on their left hand. If participants pressed 4, the task moved to the next trial. ***E:*** *Schematic of the BOLD sequence allowing artefact free combination of alpha TMS bursts.*

Magnetic Resonance Imaging & Transcranial Magnetic Stimulation

MRI images were acquired at the Magnetic Resonance Imaging facility of the Human Neuroscience Platform of the Fondation Campus Biotech Genève (FCBG, Biotech Campus, Geneva, Switzerland), using a Siemens Prisma 3 Tesla scanner (Siemens Healthineers, Germany).

Standard MRI sequences acquisition

Anatomical images were acquired with a 64-channel head and neck coil using a 3D MPRAGE sequence (TR/TE = 2300/2.96 ms, flip angle 9°, 192 sagittal slices, matrix = 256, 1x1x1 mm^3 resolution) covering the whole head. For retrospective distortion correction, static field mapping was performed with a double-echo spoiled gradient echo sequence (TR= 652 ms, TE1/TE2=4.92/7.38 ms, resolution 2.2x2.2x2.2 mm^3, whole head coverage), generating two magnitude images and one image representing the phase difference between the two echoes.

Combined TMS-fMRI sequences acquisition

For combined TMS-fMRI images, two dedicated coil arrays were used (Navarro de Lara et al., 2017). This setup consisted of an ultra-slim 7-channel receive-only coil array, which was placed between the subject's head and the TMS coil (MRi-B91, MagVenture, Farum, Denmark) and connected to a MagPro XP stimulator (MagVenture, Farum, Denmark). A second, receive-only MR coil was positioned over Cz in the EEG 10-20 system to allow a full coverage of the participant's brain.

The *Rest-TMS* and MDD *Task-TMS* sequences were acquired with a GE-EPI sequence using the same parameters: 40 axial slices, slice thickness = 2.2 mm, in-plane resolution = 2.2 mm, TR = 2000 ms, TE = 30 ms, FOV = 242 mm, flip angle = 67°, GRAPPA = 2, Multiband Factor (MB) = 2. A gap was introduced between consecutive EPI volumes in

order to guaranty artefact free MR images after TMS stimulation (Navarro de Lara et al., 2015). For both rest and task TMS sequence, a single repetition time (TR=2000 ms) was therefore composed of 40 slices acquired during 1430 ms followed by a gap of 570 ms before the next volume acquisition. The synchronization of TMS pulse was carried out with an in-house script using Matlab (R2019).

Static field mapping was also performed with the TMS-MRI coils using the same double-echo spoiled gradient echo sequence (TR = 652 ms, TE = 4.92 and 7.38 ms, slice thickness: 2.2 mm, in-plane resolution = 2.2 mm, flip angle = 60°) that generates two magnitude images and one image representing the phase difference between the two echoes.

Preprocessing of fMRI images

Statistical Parametric Mapping software (SPM12, Wellcome Department of Imaging Neuroscience, UK) was used for data pre-processing and analysis of the four datasets (*Rest TMS* and *Task TMS* datasets, on both EVA and hMT+/V5). Spatial distortions due to field inhomogeneities were removed from all EPI images using the Fieldmap toolbox from SPM12 (Andersson et al., 2001). Subsequently, all time-series were motion-corrected to the first volume using 6 degrees of freedom (3 rotations, 3 translations) and drifts in signal time courses were corrected as well. To improve the normalization procedure, two intermediate steps were added (see online materials for further details about the additional sequences used for coregistration purposes). A first co-registration was performed between the mean realigned and slice timing corrected image and the SSFP sequence acquired with the same MR coil (and thus the same spatial coverage). The resulting, co-registered image was once more co-registered to the SSFP sequence acquired with the MR coil integrated into the scanner (i.e., the body coil, thus preserving

318 the contrast). The latter could then be easily co-registered to the high resolution T1
319 image acquired with the 64-channel head coil that covered the whole brain, and later
320 transformed into standard MNI space using a segmentation-based normalization
321 approach (Ashburner and Friston, 2005). Finally, the normalized images were spatially
322 smoothed using a Gaussian kernel (4 mm, Full-width half-maximal). The realignment
323 parameters estimated during spatial pre-processing for the *Rest TMS* and *Task TMS*
324 dataset were introduced in the design matrix as regressors of no interest in order to
325 prevent confounding activations related to minor head movements during scanning. The
326 experimental event-related designs were convolved with the canonical hemodynamic
327 response function, and the resulting models described in the following section were
328 estimated using a high-pass filter at 128 s to remove low-frequency artefacts.

329

330 ***fMRI Univariate Analysis***

331 EVA and hMT+/V5 datasets were similarly analyzed using general linear models (GLM) to
332 calculate individual contrasts. For the *Task TMS* sequence, a design matrix with TMS
333 conditions (*TMS*, *noTMS*) and visual state (*Moving*, *Static*) was constructed using the
334 correct trials only. Note that to allow proper comparison between the TMS and noTMS
335 conditions, the noTMS correct trials were shuffled at the individual level. There were on
336 average 25(+/- 6) (correct) moving trials for each of the TMS and noTMS condition and
337 31(+/- 8) (correct) static trials for each of the TMS and noTMS condition. For the group
338 analysis, paired-t-tests were conducted to assess the effect of TMS (*TMS* versus *noTMS*),
339 *and the visual state (Moving* versus *Static)*.

340 For the *RestTMS* sequence, we defined a design matrix comprising three conditions
341 (*HighTMS*, *LowTMS* and *noTMS*). T-contrasts for each TMS condition were established
342 for all participants. For the purpose of this study, we only contrasted *HighTMS* versus

343 *noTMS* using a paired-t-test at the group level. The statistical significance threshold was
344 set to a height threshold of $p < 0.001$ uncorrected, at the voxel level and to that of $p <$
345 0.05 at the cluster level after false-discovery rate (FDR) correction. Group analyses were
346 conducted using the GLMFlex Fast2 toolbox
347 (https://habs.mgh.harvard.edu/researchers/data-tools/glm-flex-fast2/).

348 To explore the effects of TMS across conditions within the stimulated regions
349 EVA and hMT+/V5, mean beta values were extracted from regions of interest (ROIs)
350 defined as a 8 mm radius sphere based on the results of the group-level analysis of the
351 motion processing localizer described above using the MarsBaR toolbox (Brett et al.,
352 2002)(right EVA: 6, -83, 11 and right hMT+/V5: 58, -66, -3). For each site of stimulation
353 (EVA and hMT+/V5) in the *Task TMS* condition, repeated measure ANOVAs were built
354 with TMS and visual stimulus as within-subject factors. Planned comparisons between
355 TMS and noTMS were conducted if significant interactions were reported in order to
356 clarify the directionality of the results. For the *Rest TMS* condition, paired-t-tests were
357 applied between TMS and noTMS conditions.

358

359 ***fMRI Multivariate Analysis:***

360 Independent Component Analysis (ICA) was used on the motion discrimination task data
361 to estimate independent spatiotemporal functional networks from the data and to
362 visualize networks specifically modulated by TMS. ICA uses fluctuations in BOLD signal to
363 split it into maximally independent spatial maps or components, each explaining a
364 unique part of variance from the 4D fMRI data. Then, all components have their specific
365 time course related to a coherent neural signal potentially associated with intrinsic brain
366 networks, artifacts, or both. The group ICA of fMRI Toolbox (GIFT version 3.0b; (Calhoun
367 et al., 2001)) was used. First, it concatenates the individual data followed by the

368 computation of subject-specific components and time course. Maximum Description
369 Length (MDL) and Akaike's criteria were applied to estimate the number of ICs in our
370 data. Using principal component analysis, individual data was reduced. Then, the
371 informax algorithm (Bell and Sejnowski, 1995) was applied for the group ICA and
372 estimated 16 components. In order to improve the IC's stability, the ICASSO was applied
373 and run 20 times (Himberg et al., 2004). Over the 16 extracted network components, we
374 focused on the TMS specific networks defined by the overlap between the activated
375 clusters and the coordinates of the stimulation target. Based on these independent
376 components, we then examined how each condition (Moving or Static) covaries with the
377 TMS networks using the *temporal sorting* option in the GIFT toolbox. Temporal sorting
378 consists in regressing the fMRI specific time course for each individual against the design
379 matrix for the experimental conditions. The resulting betas weights represent the
380 degree to which network was recruited by the conditions. For a network, positive and
381 negative b weights indicate the level of network recruitment in each experimental
382 condition. Paired-sample t-tests were used to identify networks that were significantly
383 modulated by TMS at rest and during motion discrimination using $p < 0.05$.

384 ***Brain Networks generation and Graph Theoretical Analysis***

385 In addition to ICA, we used the graph theoretical network analysis toolbox GRETNA to
386 image connectomics and construct the functional brain networks derived from the full
387 $TaskTMS_{(EVA)}$ and $TaskTMS_{(hMT+/V5)}$ dataset *comprising all the conditions of interest (e.g.,*
388 *noTMS, TMS, motion or static stimuli)."* (Wang et al., 2015). The whole brain was
389 divided into 90 cortical and subcortical regions according to Automated Anatomical
390 Labeling (Tzourio-Mazoyer et al., 2002), and the mean time series for each of the 90
391 regions was extracted. Pearson's correlation coefficients for each pair of regions were
392 calculated for the mean time series of all of the 90 regions, and z-transformed using

Fisher's Z transformation. Subsequently, a positive binary undirected connection functional network was constructed according to a range of selected threshold of the relation matrix. As there is no defined standard for threshold selection in the construction of a binary connection brain functional network, sparsity was used as a range of correlation coefficient thresholds for correlation metrics. It was defined as the existing number of edges in a graph divided by the maximum possible number of edges. In accord with previous studies, we set both the sparsity and Pearson correlation threshold of the functional network to range from 0.05 to 0.5 (in 0.05 steps), resulting in a more efficient functional network than a random network with the number of artificial edges minimized (Achard and Bullmore, 2007) (Zhao et al., 2017). Graph theoretical analysis was applied to assess the topological and organizational properties focusing on 3 graph theoretical metrics (Rubinov and Sporns, 2010). These metrics were: the clustering coefficient (λ), which measures how much neighbors of a node are connected to each other and is closely related to local efficiency; characteristic path length (γ), which is the average number of edges needed to get from any node in the network to any other node in the network and is inversely related to global efficiency; small worldness (δ), which reflects whether the network balances global integration and local segregation for efficient information processing (Latora and Marchiori, 2001). To compare graph theoretical network properties between EVA and hMT+/V5, integration of the topological metric over all selected ranges of sparsity values was calculated using GRETNA. Paired t-tests corrected for FDR ($p < 0.05$) were performed between the topological measures of EVA and hMT+/V5 networks.

3. Results

419 We used online TMS-fMRI coupling in healthy participants in order to perturb and map
420 the right EVA ($TMS_{(EVA)}$) and the right hMT+/V5 ($TMS_{(hMT+/V5)}$) during a motion direction
421 discrimination task (MDD-Task) and at rest. An additional offline experiment targeted
422 the right primary motor cortex ($TMS_{(M1)}$) in another subgroup of healthy participants
423 (Figure 1A-D).

424

425 **2.1 TMS over EVA and hMT+/V5 deteriorates motion direction discrimination, but not**
426 **motion perception**

427 Figure 1E shows the mean and individual motion perception accuracy (+/- SEM),
428 reflecting how well participants could distinguish between moving and static stimuli
429 when a TMS burst was applied over EVA (top row), hMT+/V5 (middle row) and over the
430 control region M1 (bottom row). A mixed ANOVA revealed no main effect of Site ($F_{(2,30)}$ =
431 2.99, $p = 0.07$, $\eta^2 = 0.107$), TMS ($F_{(1,15)} = 1.43$, $p = 0.24$, $\eta^2 = 0.009$) and no significant TMS
432 by Site interaction ($F_{(2,15)} = 0.8$, $p = 0.462$, $\eta^2 = 0.023$), suggesting that TMS has no
433 consequence on motion perception in these three regions. In contrast, the same model
434 on motion direction discrimination performances revealed a significant TMS effect ($F_{(1,15)}$
435 $= 27.46$, $p < 0.001$, $\eta^2 = 0.251$) and Site effect ($F_{(2,30)} = 10.3$, $p < 0.001$, $\eta^2 = 0.13$). There
436 was also a TMS by Site interaction ($F_{(2,30)} = 13.85$, $p < 0.001$, $\eta^2 = 0.14$), driven by an
437 absence of TMS effect for M1 ($t(15) = -0.2$, $p = 1$) compared to marked decays in
438 performance when TMS was applied to EVA ($t(15) = 5.6$, $p < 0.001$) and hMT+/V5 ($t(15)$ =
439 5.4, $p < 0.001$) (Figure 1F). Importantly, baseline performance (noTMS conditions) was
440 similar across sites ($F(2,30) = 0.112$, $p = 0.894$).

441 We next examined the relationship between awareness and accuracy by taking into
442 account motion awareness ratings (Figure 1G). Without TMS, motion direction
443 discrimination increased (moved away from chance level) as subjective awareness of

motion increased. This indicates that without TMS, performance is tied to conscious motion awareness. The rmANOVA with TMS and Rating as within subject factors revealed a significant interaction only for $TMS_{(EVA)}$ ($F(3,45) = 8.21$, $p < 0.001$, $\eta^2 = 0.129$) and $TMS_{(hMT+/V5)}$ ($F(3,45) = 3.4$, $p = 0.026$, $\eta^2 = 0.069$) compared to $TMS_{(M1)}$ ($F(3,12) = 1.18$, $p = 0.36$, $\eta^2 = 0.049$).

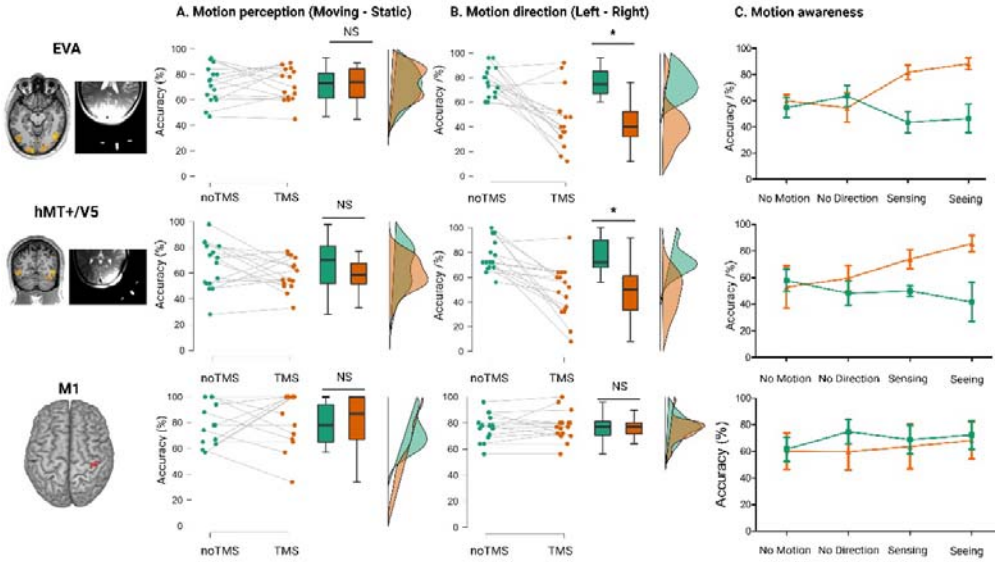

Figure 2: A: Individual data, box plots and smoothed density histograms of motion perception with and without TMS *for* $TMS_{(EVA)}$ *(top row),* $TMS_{(hMT+/V5)}$ *middle row) and* $TMS_{(M1)}$ *(bottom row);* ***B: Individual, group average and distribution of motion direction discrimination with and without TMS*** *for* $TMS_{(EVA)}$ *(top row),* $TMS_{(hMT+/V5)}$ *(middle row) and* $TMS_{(M1)}$ *(bottom row);* ***C: Relationship between behavioural accuracy and awareness of motion*** *with TMS (in green) or without TMS (in orange) for* $TMS_{(EVA)}$ *(top row),* $TMS_{(hMT+/V5)}$ *(middle row) and* $TMS_{(M1)}$ *(bottom row).*

Noteworthily, when comparing TMS at early versus late onsets, performances were significant different for $TMS_{(EVA)}$ ($t_{(9)} = -3.15$, $p = 0.034$) but not for $TMS_{(hMT+/V5)}$ ($t_{(9)} = -1.6$, $p = 1$), suggesting that interfering with recurrent feedbacks loops only impaired motion direction discrimination in hMT+/V5. Performances for $TMS_{(M1)}$ were unchanged ($t_{(9)} = -0.64$, $p = 1$) (Supplementary Figure S1).

2.2 Local brain effects of TMS

465 *2.2.1 TMS induces negative BOLD responses at rest*

466 At rest, the fMRI contrast TMS_{-RS} versus $noTMS_{-RS}$ revealed local suppressive effects for
467 both EVA (Figure 2A, left panel) and hMT+/V5 stimulation (Figure 2B, left panel). Regions
468 of Interest (ROI) created from the functional localizer, confirmed the local deactivation
469 underneath the coil (TMS_{-RS} *versus* $noTMS_{-RS}$ EVA: $t_{(15)} = 4.47$, $p = 0.0004$, Cohen's d: -
470 1.12, Figure 2C, left panel, hMT+/V5: $t_{(15)} = 2.06$, $p = 0.049$, Cohen's d: -0.6,Figure 2D,
471 left panel). Note that whole-brain analysis for $TMS_{(EVA)}$ showed additional decreased
472 regional activity in the ipsilateral hMT+/V5 and positive activation in the supplementary
473 motor area (SMA) and the frontal eye field (FEF). $TMS_{(hMT+/V5)}$ also revealed a negative
474 cluster in the ipsilateral EVA, and in the frontal eye field (FEF) (see Supplementary Tables
475 S1 and S2).

476

477 *2.1.3 TMS suppresses BOLD activity during motion processing*

478 When participants were presented with moving stimuli, both TMS sites induced a
479 significant local decrease in BOLD activity (Figure 3A, middle panel for EVA and Figure
480 3B, middle panel for hMT+/V5, and see Supplementary Tables S3 and S4). Interestingly,
481 the same contrast on the correct static trials did not reveal any significant TMS effect
482 (Figure 3A for EVA and Figure 3B for hMT+/V5, right panels).

483 The rmANOVA modeling the beta estimates for $TMS_{(EVA)}$ showed a main effect of TMS
484 ($F_{(1,12)} = 6.32$, $p = 0.03$, $\eta^2 = 0.102$) and a significant TMS by Visual stimulus (moving or
485 static) interaction ($F_{(1,12)} = 10.82$, $p = 0.006$, $\eta^2 = 0.113$), while no main effect of Visual
486 stimulus was found ($F_{(1,12)} = 3.93$, $p = 0.07$, $\eta^2 = 0.115$). Post hoc comparisons between
487 TMS and noTMS for the two visual conditions revealed a significant decrease in beta
488 estimates for moving stimuli only (moving: $t_{(12)} = 7.03$, $p < 0.001$, Cohen's d = 1.88 ,
489 static: $t_{(12)} = -0-079$, $p = 0.94$, Cohen's d = -0.02). The same rmANOVA for $TMS_{(hMT+/V5)}$

only revealed a significant TMS by Visual stimulus interaction ($F_{(1,14)} = 6.1$, $p = 0.03$, $\eta^2 = 0.08$). The main effects were not significant (TMS: $F_{(1,14)} = 3$, $p = 0.11$, $\eta^2 = 0.071$; Visual stimulus: $F_{(1,14)} = 1.11$, $p = 0.31$, $\eta^2 = 0.025$). Post hoc comparisons between TMS and noTMS in the two visual conditions confirmed a significant decrease in beta weights for the TMS condition associated with moving stimuli ($t_{(14)} = -3.73$, $p = 0.002$, Cohen's d = -0.964) , but not with static stimuli ($t_{(14)} = 0.058$, $p = 0.954$, Cohen's d = 0.015).

Finally, to investigate the link between the TMS-induced impairments in motion direction discrimination and the reduction in local activation, we performed planned correlation analyses. We found no significant correlation in EVA ($r = -0.41$, $p = 0.14$), but a significant positive association between the amount of task impairment and the strength of the deactivation in hMT+/V5 ($r = 0.82$, $p<0.001$) (Figure 3E & 2F).

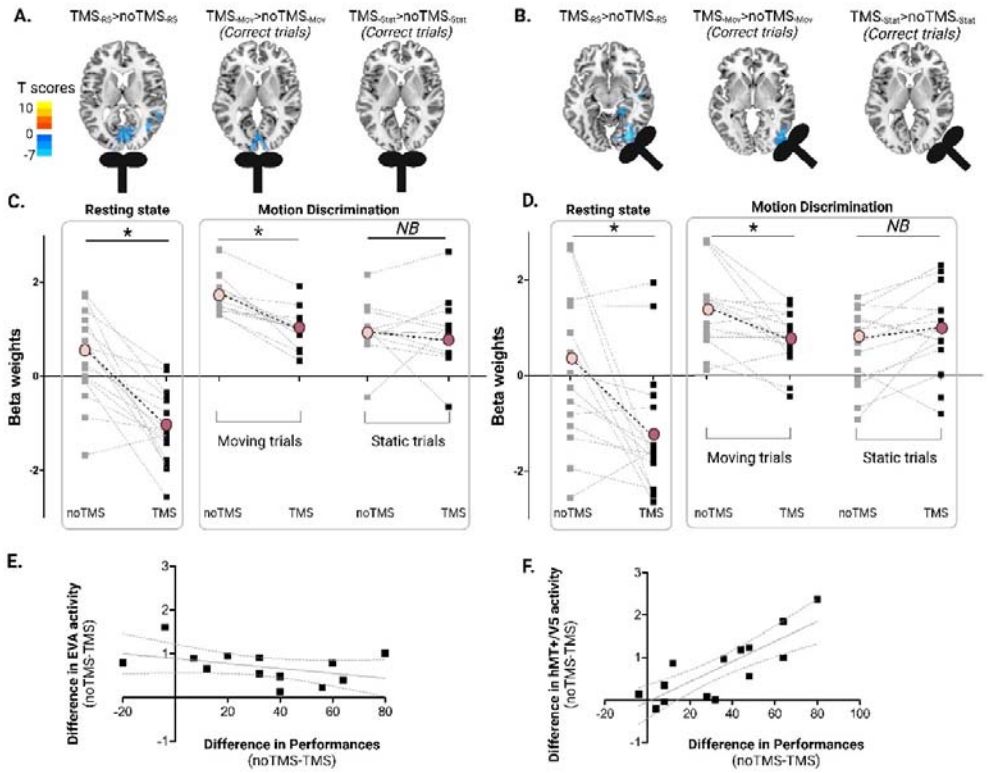

Figure 3: Local effects of TMS: A*: Activation maps corresponding to the TMS > noTMS contrast at rest (right panel), simultaneously to moving visual stimuli (middle panel), simultaneously to static visual stimuli (right panel) for* $TMS_{(EVA)}$*;* ***B:*** *Activation maps corresponding to the TMS > noTMS contrast at rest (right panel), simultaneously to moving visual stimuli (middle panel), simultaneously to static visual stimuli (right panel) for* $TMS_{(hMT+/V5)}$*;* ***C:*** *ROI analysis associated with*

the $TMS_{(EVA)}$ > $noTMS_{(EVA)}$ contrast at rest, while presenting moving stimuli and static visual stimuli; ***D****: ROI analysis associated with the $TMS_{(hMT+/V5)}$ > $noTMS_{(hMT+/V5)}$ contrast at rest, while presenting moving stimuli, while presenting static visual stimuli;* ***E:*** *Relationship between impaired motion direction discrimination and deactivation in EVA for $TMS_{(EVA)}$; $TMS_{(hMT+/V5)\text{-}Mov}$ > $TMS_{(hMT+/V5)\text{-}Stat}$ ROI analysis;* ***F:*** *Relationship between impaired motion direction discrimination and deactivation in hMT+/V5 for $TMS_{(hMT+/V5)\text{-}Mov}$. Please note the strong correlation between $TMS_{(hMT+/V5)}$ related changes in behavior and $TMS_{(hMT+/V5)}$ -related changes in BOLD activity (r = 0.82, p<0.001).*

3.2 Multivariate and graph theory-based network analysis

We further investigated whether and how long-range brain activity was modulated by TMS over *EVA* or *hMT+/V5* during motion direction discrimination. We first applied an independent component analysis to extract hidden spatiotemporal components contained within the $TMS_{(EVA)}$ and $TMS_{(hMT+/V5)}$ task data. Second, we applied a graph theoretical analysis to assess the topological and organizational properties of these networks.

3.2.1 $TMS_{(EVA)}$ networks

The ICA applied to the $TMS_{(EVA)}$ data at rest revealed 16 components, among which 13 were considered as functional brain networks and three components considered as noise. Three networks (IC1, IC3 and IC14) were labelled as TMS-related networks because they overlapped with the stimulation site and were significantly modulated by TMS (Figure 4A, Supplementary Figure S2 for all the other functional brain networks and Supplementary Table S5 for the MNI coordinates). Interestingly, those three networks only encompassed the stimulated EVA area. The temporal regression analysis applied to the components' time courses showed that they were significantly down regulated by $TMS_{(EVA)}$ only when considering moving stimuli (IC1: $t_{(15)}$ =4.9, p_{cor} = 0.006, Cohen's d: 1.02, IC3: $t_{(15)}$ = 2.41, p_{cor} = 0.039, Cohen's d: 0.6, IC14: $t_{(15)}$ = 2.25, p_{cor} = 0.051, Cohen's d: 0.56, Figure 3A). In contrast, IC14 was over-expressed when

536 associated with static stimuli (IC14: $t_{(15)}$=3.6, p_{cor} = 0.005, Cohen's d: 0.45). The other two
537 IC were not significantly modulated by TMS during static stimuli (IC1: $t_{(15)}$ = 0.89, p_{cor} = 1,
538 Cohen's d: 0.09, IC3: $t_{(15)}$ = 1.3, p_{cor} = 0.21, Cohen's d: 0.32).

539

540 *3.2.2 $TMS_{(hMT+/V5)}$ networks*

541 Among the 14 (out of 16) components representing functional brain networks for
542 $TMS_{(hMT+/V5)}$ (see Supplementary Figure S3 and Supplementary Table S6), three
543 corresponded to TMS networks (IC5, IC7, IC13, Figure 4B). Compared to $TMS_{(EVA)}$, these
544 networks were more diffused, comprising the stimulated right hMT+/V5 area, the
545 bilateral or contralateral left FEF (IC5 and IC7), the medial prefrontal cortex and pre-
546 supplementary motor area (preSMA) (IC5) and the posterior parietal cortex (PPC) (IC13).
547 The temporal regression analysis applied to the components' time courses showed that
548 IC5 and IC13 were suppressed by TMS when associated with moving stimuli (IC5: $t_{(14)}$ =
549 2.5 p_{cor} = 0.07, Cohen's d: 0.63, IC7: $t_{(14)}$ = 0.35 p_{cor} = 0.73, Cohen's d: 0.7, IC13:$t_{(14)}$ = 2.6
550 p_{cor} = 0.048, Cohen's d: 0.62, Figure 4B) and IC7 showed a trend toward an up-regulated
551 with static stimuli (IC7: $t_{(14)}$ = 2.2 p_{cor} = 0.07, Cohen's d: 0.57, IC5: $t_{(14)}$ = 1.3 p_{cor} = 0.315,
552 Cohen's d: 0.33, IC13: $t_{(14)}$ = 0.47 p_{cor} = 0.774, Cohen's d: 0.12).

553

554 *3.2.3 Graph-based network analysis*

555 We applied a graph theory approach to compare the topological organization of the
556 functional connectivity networks, when EVA or hMT+/V5 was perturbed during motion
557 discrimination. We first investigated small-world topological properties especially
558 because networks with high small-world properties are believed to play a role in
559 protecting the brain from local perturbation or damage. Both EVA and hMT+/V5

networks exhibited small-world properties ($\lambda \approx 1$ and $\sigma > 1$) among the selected sparsity values (see Methods section). Interestingly, there was a significant difference in the small-world network parameters (σ) between EVA networks and hMT+/V5 networks with higher σ for EVA networks at the sparsity values 0.3, 0.4, 0.45 and marginally at 0.35 (see supplementary Table S7 for all paired t-tests), also considering the mean across all spasticity values ($t_{(14)} = 2.9$, $p = 0.034$, Cohen's d: -0.67) (Figure 4C). There was no significant difference in normalized clustering coefficient (λ) between the two networks ($t_{(14)} = 0.42$, $p = 0.68$, Cohen's d: 0.12). Finally, characteristic path length (γ) showed a significant increase at sparsity thresholds of 0.2, 0.25 and marginally at 0.15 (Figure 4D and see Supplementary Table S8 for all paired t-tests). The difference between EVA and hMT+/V5 networks was also significant across all sparsities ($t_{(14)} = 2.9$, $p = 0.012$, Cohen's d: 0.75) (Figure 4E and see supplementary Table S9 for all paired t-tests).

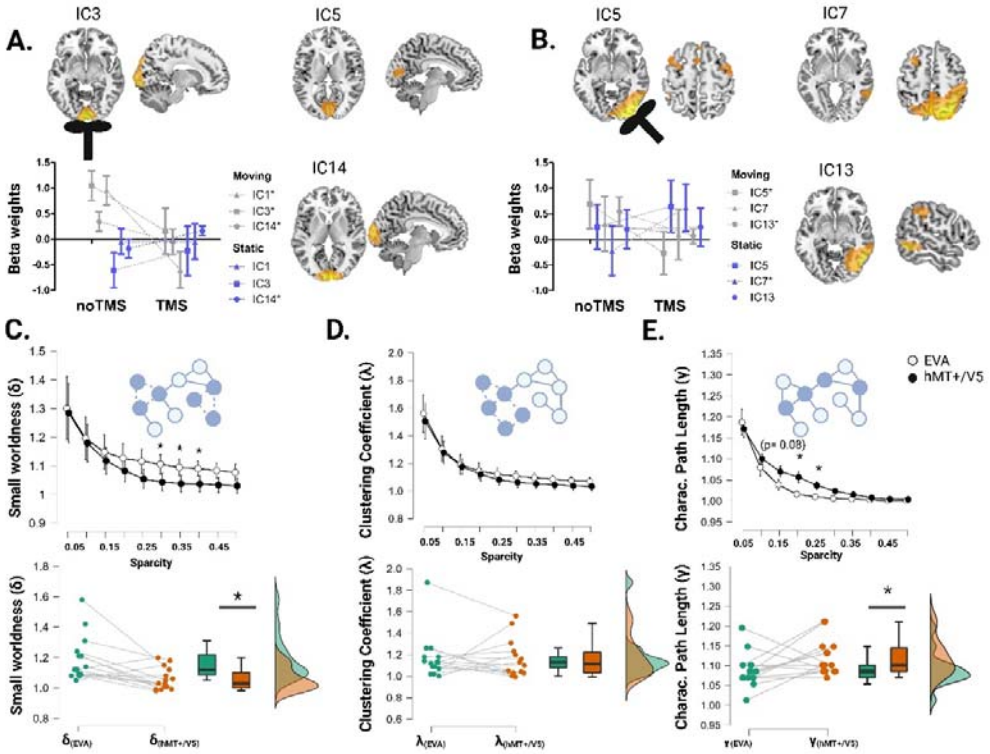

***Figure 4A**: $TMS_{(EVA)}$-specific component networks that are modulated by TMS during motion discrimination and temporal regression analysis for the noTMS and $TMS_{(EVA)}$ conditions associated with moving or static stimuli; **B:** $TMS_{(hMT+/V5)}$-specific component networks that are modulated by TMS during motion discrimination and temporal regression analysis for the noTMS and $TMS_{(EVA)}$ conditions associated with moving or static stimuli; **C**: Small-worldness properties for $TMS_{(EVA)}$ and $TMS_{(hMT+/V5)}$ along the sparsity threshold of 0.05-0.50 (top row) and mean values (bottom row); **D:** Clustering coefficient for $TMS_{(EVA)}$ and $TMS_{(hMT+/V5)}$ along the sparsity threshold of 0.05-0.50 (top row) and mean values (bottom row); **E:** Characteristic Path Length properties for $TMS_{(EVA)}$ and $TMS_{(hMT+/V5)}$ along the sparsity threshold of 0.05-0.50 (top row) and mean values (bottom row); * p(FDR) < 0.05.*

586 # 4. Discussion

587 This study used short bursts of 10Hz TMS to disrupt either a low-level visual area
588 (EVA) or a highly specialized, motion sensitive, visual area (hMT+/V5) during concurrent
589 fMRI. We first confirmed targets causal engagement with significant TMS task
590 impairments that were specific to motion direction discrimination. We also describe a
591 local context-dependent BOLD deactivation common to both areas, but only predictive
592 of task impairment when TMS was applied to hMT+/V5. Finally, our results revealed
593 distinct topological networks' adaptations in response to TMS perturbation of the EVA
594 or hMT+/V5, possibly reflecting different levels of networks resilience to the focal lesion.

595 In line with the concept of "virtual lesion" described in the literature (Pascual-
596 Leone et al., 1999), the TMS bursts applied to either EVA and hMT+/V5, resulted in a
597 selective and transient deterioration of performance of a left/right motion direction
598 discrimination task. This was interpreted to reflect successful causal and selective
599 disruption of brain functioning. Interestingly, participants remained able to dissociate
600 moving from static stimuli. This dissociation is likely supported by the existence of
601 independent substrates supporting unspecific motion processing versus global motion
602 direction integration in EVA and hMT+/V5 (Simoncelli and Heeger, 1998). There is
603 evidence showing that a sub-population of neurons in hMT+/V5 focuses on the
604 processing of local motion signals similar to that in EVA, and some other neuronal
605 populations rather process global motion (Born and Tootell, 1992). Our TMS disruption
606 might have specifically impacted on the neurons in charge of the decoding of motion
607 directions. Furthermore, other areas of the motion processing network, not directly
608 impaired by the focal perturbation, such as the medial superior temporal area (MST)
609 (Sclar et al., 1990) might be involved in unspecific motion processing, explaining the lack
610 of impairment. Considering now the relationship between motion awareness and

motion direction discrimination, we found that the direction of the moving trials that were judged as “moving”, were not correctly guessed when both areas were stimulated. In contrast, “unaware” trials were unchanged. We can speculate that this residual, unconscious ability of detecting changes in the dots’ positions might be at least partially supported by the activation of the fast, direct geniculo-extra-striate pathway (Abed Rabbo et al., 2015) (Bridge et al., 2008) (Ajina et al., 2015).

Locally, motion direction discrimination was associated with an increase in EVA and hMT+/V5 BOLD activity, probably representing the populations of neurons tuned to the presented direction of motion since only the correct trials were considered. In contrast, the selective behavioral impairment induced by TMS was associated with a local loss of BOLD signal strength only when participants were judging motion direction. This *signal suppression* effect fits with the traditional use of temporary virtual lesions in a healthy brain, where TMS would inhibit the activity of active neuronal populations, specifically in this study, the neurons coding for on-axis directions. Consequently, the signal-to-noise ratio for properly integrating the encoding properties of the remaining active motion sensitive neurons got significantly worsened, explaining the deterioration of performance. This is further supported by the significant correlation between the level of impairment and the amount of hMT+/V5 BOLD suppression. Finally, this finding is perfectly in line with extracellular recordings in monkeys showing strong associations between neuronal responses and accuracy depending on the difference between the stimulus motion and the preferred direction of a neuron (Purushothaman and Bradley, 2005) (Cohen and Newsome, 2009). Therefore, we conclude that our findings provide neuroimaging evidence that active rescaling of local BOLD activation makes TMS more likely to specifically suppress the active neurons.

This BOLD suppression occurred locally on the targeted region, but also remotely via functional coupling at the network level. TMS networks were specifically down-regulated when participants were presented with moving stimuli for both $TMS_{(EVA)}$ and $TMS_{(hMT+/V5)}$. Conversely to local activation, the static condition led to an up-regulation of some TMS networks, confirming that multivariate network analyses might be more sensitive to contextual changes than classical univariate analyses (Hebart and Baker, 2018) (Brauchli et al., 2019) and might be associated with attentive compensatory mechanisms (Parks and Madden, 2013).

Another observation arising from the ICA analysis was that TMS networks' configurations were significantly different whether TMS was applied to EVA or hMT+/V5. We found that the $TMS_{(hMT+/V5)}$ networks were spatially more distributed, including additional associative areas, such as the frontal eye field (FEF), the posterior parietal cortex (PPC) or the medial prefrontal cortex (mPFC). In comparison, the independent components forming the $TMS_{(EVA)}$ networks were restricted to the stimulated EVA. To quantify these observations, we used graph-based theory analyses and found that whole-brain functional networks were different whether EVA or hMT+/V5 was perturbed. Specifically, EVA networks showed higher small-worldness values, characterized by local clustering of elements and short path lengths, compared to $TMS_{(hMT+/V5)}$ networks. The $TMS_{(EVA)}$ networks configuration appears to support efficient parallel information processing, which typically maximizes information transfer efficiency at a relatively low wiring cost (Achard and Bullmore, 2007). Then, it is possible that the clustered $TMS_{(EVA)}$ networks enable flexible redistribution of network activity, to maintain an orchestrated network stability despite various internal and external perturbations (Wu et al., 2019). In contrast, the existence of the scattered functional $TMS_{(hMT+/V5)}$ networks adaptation might reflect propagation of task-specific suppression that is distributed over higher visual brain regions (FEF, PPC or mPFC). These suppressed,

661 broader effects might prevent compensation or re-balancing of network activity in
662 response to a lesion or a focal perturbation.

663 Although this difference in network adaptation between $TMS_{(EVA)}$ and
664 $TMS_{(hMT+/V5)}$ did not translate into a behavioural difference using these TMS and task
665 parameters, our results are in congruence with a modelling study, showing that brain
666 hubs, where activity is integrated and further distributed (like EVA in our case) operate
667 in a slower regime and appear to be functionally less affected by focal perturbations
668 (Gollo et al., 2017). In contrast, perturbations of peripheral or more associative areas
669 (e.g., hMT+/V5), might have greater impact on acute network activity. Lesion studies
670 also provided evidence that damage to the homologue of hMT+/V5 in behaving cats
671 impairs more relearning of motion discrimination and learning transfer than lesions to
672 EVA (Das et al., 2012). Our control experiment using later TMS onsets also shows
673 detrimental behavioural effects only for hMT+/V5 stimulation. To sum up, the network
674 analyses revealed differences between the two disrupted areas, not observable with
675 classical activation analyses. Perturbating a highly specialized region such as hMT+/V5 in
676 this case, led to more widespread effect, leading to the conclusion that this region is
677 more vulnerable to focal perturbation.

678 In conclusion, despite growing interest and extensive computational modelling
679 contributions, the causal mechanisms underlying neural network dynamics after a
680 lesion, remain elusive. In the present study, we used concurrent TMS-fMRI coupling as a
681 tool to probe neural mechanisms underlying functional reorganization of whole-brain
682 dynamics using a "virtual-lesion" approach. First, we provide neuroimaging evidence for
683 task selectivity of TMS effects, which is more prompt to act on active neurons
684 specifically. We also demonstrate that selective, focal virtual lesions can result in distinct
685 dis-regulations in visual network activity, depending on which hierarchical level is

686 perturbed. Complementarily to lesion studies (Das et al., 2012), these findings motivate
687 the use of TMS-fMRI coupling as an additional tool to assess 'disconnectomics' and their
688 network and behavioural effects after brain lesions (Egger et al., 2021). This technique
689 could be leveraged to precisely map how a local perturbation propagates to large-scale
690 behavioural deficits by comparing the neural impact of TMS-induced virtual lesion
691 during different active cognitive processes.

692

Acknowledgements:

We thank Holly Bridge for her insightful comments on the manuscript. We would like to thank the MRI and neuromodulation facilities of the Human Neuroscience Platform of the Fondation Campus Biotech Geneva, for technical advice. This study was supported by the Bertarelli Foundation (Catalyst BC77O7 to FCH & ER), by the Swiss National Science Foundation (PRIMA PR00P3_179867 to ER), and by the Defitech Foundation (to FCH).

Conflict of interest statement: The authors declare no financial or non-financial competing interests.

References

Abed Rabbo, F., Koch, G., Lefèvre, C., Seizeur, R., 2015. Direct geniculo-extrastriate pathways: a review of the literature. Surg. Radiol. Anat. SRA 37, 891–899. https://doi.org/10.1007/s00276-015-1450-7

Achard, S., Bullmore, E., 2007. Efficiency and cost of economical brain functional networks. PLoS Comput. Biol. 3, e17. https://doi.org/10.1371/journal.pcbi.0030017

Ajina, S., Pestilli, F., Rokem, A., Kennard, C., Bridge, H., 2015. Human blindsight is mediated by an intact geniculo-extrastriate pathway. eLife 4, e08935. https://doi.org/10.7554/eLife.08935

Amassian, V.E., Cracco, R.Q., Maccabee, P.J., Cracco, J.B., Rudell, A., Eberle, L., 1989. Suppression of visual perception by magnetic coil stimulation of human occipital cortex. Electroencephalogr. Clin. Neurophysiol. Potentials Sect. 74, 458–462. https://doi.org/10.1016/0168-5597(89)90036-1

Andersson, J.L.R., Hutton, C., Ashburner, J., Turner, R., Friston, K., 2001. Modeling Geometric Deformations in EPI Time Series. NeuroImage 13, 903–919. https://doi.org/10.1006/nimg.2001.0746

Ashburner, J., Friston, K.J., 2005. Unified segmentation. NeuroImage 26, 839–851. https://doi.org/10.1016/j.neuroimage.2005.02.018

Bancroft, T.D., Hogeveen, J., Hockley, W.E., Servos, P., 2014. TMS-induced neural noise in sensory cortex interferes with short-term memory storage in prefrontal cortex. Front. Comput. Neurosci. 8. https://doi.org/10.3389/fncom.2014.00023

Bassett, D.S., Bullmore, E.T., 2009. Human brain networks in health and disease. Curr. Opin. Neurol. 22, 340–347. https://doi.org/10.1097/WCO.0b013e32832d93dd

Beckers, G., Hömberg, V., 1992. Cerebral visual motion blindness: transitory akinetopsia induced by transcranial magnetic stimulation of human area V5. Proc. Biol. Sci. 249, 173–178. https://doi.org/10.1098/rspb.1992.0100

Beckers, G., Homberg, V., 1992. Cerebral Visual Motion Blindness: Transitory Akinetopsia Induced by Transcranial Magnetic Stimulation of Human Area V5. Proc. Biol. Sci. 249, 173–178.

Bell, A.J., Sejnowski, T.J., 1995. An information-maximization approach to blind separation and blind deconvolution. Neural Comput. 7, 1129–1159. https://doi.org/10.1162/neco.1995.7.6.1129

Bergmann, T.O., Varatheeswaran, R., Hanlon, C.A., Madsen, K.H., Thielscher, A., Siebner, H.R., 2021. Concurrent TMS-fMRI for causal network perturbation and proof of target engagement. NeuroImage 237, 118093. https://doi.org/10.1016/j.neuroimage.2021.118093

Bestmann S., 2008. Mapping Causal Interregional Influences With Concurrent TMS-fMRI - PubMed. Exp Brain Res.

Bestmann, S., Baudewig, J., Siebner, H.R., Rothwell, J.C., Frahm, J., 2004. Functional MRI of the immediate impact of transcranial magnetic stimulation on cortical and subcortical motor circuits. Eur. J. Neurosci. 19, 1950–1962. https://doi.org/10.1111/j.1460-9568.2004.03277.x

Billman, G.E., 2020. Homeostasis: The Underappreciated and Far Too Often Ignored Central Organizing Principle of Physiology. Front. Physiol. 11.

Born, R.T., Tootell, R.B.H., 1992. Segregation of global and local motion processing in primate middle temporal visual area. Nature 357, 497–499. https://doi.org/10.1038/357497a0

Brauchli, C., Leipold, S., Jäncke, L., 2019. Univariate and multivariate analyses of functional networks in absolute pitch. NeuroImage 189. https://doi.org/10.1016/j.neuroimage.2019.01.021

Brett, M., Anton, J.L., Valabrgue, R., Poline, J.-B., 2002. Region of interest analysis using an SPM toolbox. Presented at the 8th International Conference on Functional Mapping of the Human Brain, June 2-6, 2002, Sendai, Japan. Neuroimage 13, 210–217.

Bridge, H., Thomas, O., Jbabdi, S., Cowey, A., 2008. Changes in connectivity after visual cortical brain damage underlie altered visual function. Brain J. Neurol. 131, 1433–1444. https://doi.org/10.1093/brain/awn063

Bullmore, E., Sporns, O., 2012. The economy of brain network organization. Nat. Rev. Neurosci. 13, 336–349. https://doi.org/10.1038/nrn3214

Calhoun, V.D., Adali, T., Pearlson, G.D., Pekar, J.J., 2001. A method for making group inferences from functional MRI data using independent component analysis. Hum. Brain Mapp. 14, 140–151. https://doi.org/10.1002/hbm.1048

Cocchi, L., Sale, M.V., L Gollo, L., Bell, P.T., Nguyen, V.T., Zalesky, A., Breakspear, M., Mattingley, J.B., 2016. A hierarchy of timescales explains distinct effects of local inhibition of primary visual cortex and frontal eye fields. eLife 5, e15252. https://doi.org/10.7554/eLife.15252

Cohen, M.R., Newsome, W.T., 2009. Estimates of the Contribution of Single Neurons to Perception Depend on Timescale and Noise Correlation. J. Neurosci. 29, 6635–6648. https://doi.org/10.1523/JNEUROSCI.5179-08.2009

d'Alfonso, A.A., van Honk, J., Schutter, D.J., Caffé, A.R., Postma, A., de Haan, E.H., 2002. Spatial and temporal characteristics of visual motion perception involving V5 visual cortex. Neurol. Res. 24, 266–270. https://doi.org/10.1179/016164102101199891

Das, A., DeMagistris, M., Huxlin, K.R., 2012. Different Properties of Visual Relearning after Damage to Early Versus Higher-Level Visual Cortical Areas. J. Neurosci. 32, 5414–5425. https://doi.org/10.1523/JNEUROSCI.0316-12.2012

Denslow, S., Lomarev, M., George, M.S., Bohning, D.E., 2005. Cortical and subcortical brain effects of transcranial magnetic stimulation (TMS)-induced movement: an interleaved TMS/functional magnetic resonance imaging study. Biol. Psychiatry 57, 752–760. https://doi.org/10.1016/j.biopsych.2004.12.017

Egger, P., Evangelista, G.G., Koch, P.J., Park, C.-H., Levin-Gleba, L., Girard, G., Beanato, E., Lee, J., Choirat, C., Guggisberg, A.G., Kim, Y.-H., Hummel, F.C., 2021. Disconnectomics of the Rich Club Impacts Motor Recovery After Stroke. Stroke STROKEAHA120031541. https://doi.org/10.1161/STROKEAHA.120.031541

Fornito, A., Zalesky, A., Breakspear, M., 2015. The connectomics of brain disorders. Nat. Rev. Neurosci. 16, 159–172. https://doi.org/10.1038/nrn3901

Giese, M.A., Poggio, T., 2003. Neural mechanisms for the recognition of biological movements. Nat. Rev. Neurosci. 4, 179–192. https://doi.org/10.1038/nrn1057

Gollo, L.L., Roberts, J.A., Cocchi, L., 2017. Mapping how local perturbations influence systems-level brain dynamics. NeuroImage 160, 97–112. https://doi.org/10.1016/j.neuroimage.2017.01.057

Grasso, P.A., Làdavas, E., Bertini, C., Caltabiano, S., Thut, G., Morand, S., 2018. Decoupling of Early V5 Motion Processing from Visual Awareness: A Matter of Velocity as Revealed by Transcranial Magnetic Stimulation. J. Cogn. Neurosci. 30, 1517–1531. https://doi.org/10.1162/jocn_a_01298

Grossberg, S., Mingolla, E., Pack, C., 1999. A neural model of motion processing and visual navigation by cortical area MST. Cereb. Cortex N. Y. N 1991 9, 878–895. https://doi.org/10.1093/cercor/9.8.878

Harris, J.A., Clifford, C.W.G., Miniussi, C., 2008. The functional effect of transcranial magnetic stimulation: signal suppression or neural noise generation? J. Cogn. Neurosci. 20, 734–740. https://doi.org/10.1162/jocn.2008.20048

Hebart, M.N., Baker, C.I., 2018. Deconstructing multivariate decoding for the study of brain function. NeuroImage 180, 4–18. https://doi.org/10.1016/j.neuroimage.2017.08.005

Himberg, J., Hyvärinen, A., Esposito, F., 2004. Validating the independent components of neuroimaging time series via clustering and visualization. NeuroImage 22, 1214–1222. https://doi.org/10.1016/j.neuroimage.2004.03.027

Jung, J., Bungert, A., Bowtell, R., Jackson, S.R., 2020. Modulating Brain Networks With Transcranial Magnetic Stimulation Over the Primary Motor Cortex: A Concurrent TMS/fMRI Study. Front. Hum. Neurosci. 14. https://doi.org/10.3389/fnhum.2020.00031

Koivisto, M., Leino, K., Pekkarinen, A., Karttunen, J., Railo, H., Hurme, M., 2021. Transcranial magnetic stimulation (TMS)-induced Blindsight of Orientation is Degraded Conscious Vision. Neuroscience. https://doi.org/10.1016/j.neuroscience.2021.08.025

Koivisto, M., Mäntylä, T., Silvanto, J., 2010. The role of early visual cortex (V1/V2) in conscious and unconscious visual perception. NeuroImage 51, 828–834. https://doi.org/10.1016/j.neuroimage.2010.02.042

Lamme, V.A., 2001. Blindsight: the role of feedforward and feedback corticocortical connections. Acta Psychol. (Amst.) 107, 209–228. https://doi.org/10.1016/s0001-6918(01)00020-8

Lamme, V.A., Roelfsema, P.R., 2000. The distinct modes of vision offered by feedforward and recurrent processing. Trends Neurosci. 23, 571–579. https://doi.org/10.1016/s0166-2236(00)01657-x

Latora, V., Marchiori, M., 2001. Efficient behavior of small-world networks. Phys. Rev. Lett. 87, 198701. https://doi.org/10.1103/PhysRevLett.87.198701

Leitão, J., Thielscher, A., Tünnerhoff, J., Noppeney, U., 2015. Concurrent TMS-fMRI Reveals Interactions between Dorsal and Ventral Attentional Systems. J. Neurosci. 35, 11445–11457. https://doi.org/10.1523/JNEUROSCI.0939-15.2015

Mason, R.A., Prat, C.S., Just, M.A., 2014. Neurocognitive Brain Response to Transient Impairment of Wernicke's Area. Cereb. Cortex N. Y. NY 24, 1474–1484. https://doi.org/10.1093/cercor/bhs423

Mineault, P.J., Khawaja, F.A., Butts, D.A., Pack, C.C., 2012. Hierarchical processing of complex motion along the primate dorsal visual pathway. Proc. Natl. Acad. Sci. 109, E972–E980. https://doi.org/10.1073/pnas.1115685109

Mullin, C.R., Steeves, J.K.E., 2013. Consecutive TMS-fMRI Reveals an Inverse Relationship in BOLD Signal between Object and Scene Processing. J. Neurosci. 33, 19243–19249. https://doi.org/10.1523/JNEUROSCI.2537-13.2013

Navarro de Lara, L.I., Tik, M., Woletz, M., Frass-Kriegl, R., Moser, E., Laistler, E., Windischberger, C., 2017. High-sensitivity TMS/fMRI of the Human Motor Cortex Using a Dedicated Multichannel MR Coil. NeuroImage 150, 262–269. https://doi.org/10.1016/j.neuroimage.2017.02.062

Navarro de Lara, L.I., Windischberger, C., Kuehne, A., Woletz, M., Sieg, J., Bestmann, S., Weiskopf, N., Strasser, B., Moser, E., Laistler, E., 2015. A novel coil array for combined TMS/fMRI experiments at 3 T. Magn. Reson. Med. 74, 1492–1501. https://doi.org/10.1002/mrm.25535

Ozdemir, R.A., Tadayon, E., Boucher, P., Momi, D., Karakhanyan, K.A., Fox, M.D., Halko, M.A., Pascual-Leone, A., Shafi, M.M., Santarnecchi, E., 2020. Individualized perturbation of the human connectome reveals reproducible biomarkers of

network dynamics relevant to cognition. Proc. Natl. Acad. Sci. 117, 8115–8125. https://doi.org/10.1073/pnas.1911240117

Pack, C.C., Born, R., 2010. Cortical Mechanisms for the Integration of Visual Motion. Senses Compr. Ref. 2, 189–218. https://doi.org/10.1016/B978-012370880-9.00309-1

Papo, D., Buldú, J.M., Boccaletti, S., Bullmore, E.T., 2014. Complex network theory and the brain. Philos. Trans. R. Soc. B Biol. Sci. 369, 20130520. https://doi.org/10.1098/rstb.2013.0520

Parks, E.L., Madden, D.J., 2013. Brain Connectivity and Visual Attention. Brain Connect. 3, 317–338. https://doi.org/10.1089/brain.2012.0139

Pascual-Leone, A., Bartres-Faz, D., Keenan, J.P., 1999. Transcranial magnetic stimulation: studying the brain-behaviour relationship by induction of "virtual lesions." Philos. Trans. R. Soc. Lond. B. Biol. Sci. 354, 1229–1238. https://doi.org/10.1098/rstb.1999.0476

Perini, F., Cattaneo, L., Carrasco, M., Schwarzbach, J.V., 2012. Occipital Transcranial Magnetic Stimulation Has an Activity-Dependent Suppressive Effect. J. Neurosci. 32, 12361–12365. https://doi.org/10.1523/JNEUROSCI.5864-11.2012

Purushothaman, G., Bradley, D.C., 2005. Neural population code for fine perceptual decisions in area MT. Nat. Neurosci. 8, 99–106. https://doi.org/10.1038/nn1373

Rafiei, F., Rahnev, D., 2022. TMS Does Not Increase BOLD Activity at the Site of Stimulation: A Review of All Concurrent TMS-fMRI Studies. eNeuro 9. https://doi.org/10.1523/ENEURO.0163-22.2022

Ricci, R., Salatino, A., Li, X., Funk, A., Logan, S., Mu, Q., Johnson, K., Bohning, D., George, M., 2012. Imaging the neural mechanisms of TMS neglect-like bias in healthy volunteers with the interleaved TMS/fMRI technique: preliminary evidence. Front. Hum. Neurosci. 6. https://doi.org/10.3389/fnhum.2012.00326

Romero, M.C., Davare, M., Armendariz, M., Janssen, P., 2019. Neural effects of transcranial magnetic stimulation at the single-cell level. Nat. Commun. 10, 2642. https://doi.org/10.1038/s41467-019-10638-7

Rossi, S., Antal, A., Bestmann, S., Bikson, M., Brewer, C., Brockmöller, J., Carpenter, L.L., Cincotta, M., Chen, R., Daskalakis, J.D., Di Lazzaro, V., Fox, M.D., George, M.S., Gilbert, D., Kimiskidis, V.K., Koch, G., Ilmoniemi, R.J., Lefaucheur, J.P., Leocani, L., Lisanby, S.H., Miniussi, C., Padberg, F., Pascual-Leone, A., Paulus, W., Peterchev, A.V., Quartarone, A., Rotenberg, A., Rothwell, J., Rossini, P.M., Santarnecchi, E., Shafi, M.M., Siebner, H.R., Ugawa, Y., Wassermann, E.M., Zangen, A., Ziemann, U., Hallett, M., 2021. Safety and recommendations for TMS use in healthy subjects and patient populations, with updates on training, ethical and regulatory issues: Expert Guidelines. Clin. Neurophysiol. 132, 269–306. https://doi.org/10.1016/j.clinph.2020.10.003

Rubinov, M., Sporns, O., 2010. Complex network measures of brain connectivity: uses and interpretations. NeuroImage 52, 1059–1069. https://doi.org/10.1016/j.neuroimage.2009.10.003

Ruff, C.C., Blankenburg, F., Bjoertomt, O., Bestmann, S., Freeman, E., Haynes, J.-D., Rees, G., Josephs, O., Deichmann, R., Driver, J., 2006. Concurrent TMS-fMRI and Psychophysics Reveal Frontal Influences on Human Retinotopic Visual Cortex. Curr. Biol. 16, 1479–1488. https://doi.org/10.1016/j.cub.2006.06.057

Ruff, C.C., Blankenburg, F., Bjoertomt, O., Bestmann, S., Weiskopf, N., Driver, J., 2008. Hemispheric Differences in Frontal and Parietal Influences on Human Occipital Cortex: Direct Confirmation with Concurrent TMS–fMRI. J. Cogn. Neurosci. 21, 1146–1161. https://doi.org/10.1162/jocn.2009.21097

Rust, N.C., Mante, V., Simoncelli, E.P., Movshon, J.A., 2006. How MT cells analyze the motion of visual patterns. Nat. Neurosci. 9, 1421–1431. https://doi.org/10.1038/nn1786

Ruzzoli, M., Marzi, C.A., Miniussi, C., 2010. The Neural Mechanisms of the Effects of Transcranial Magnetic Stimulation on Perception. J. Neurophysiol. 103, 2982–2989. https://doi.org/10.1152/jn.01096.2009

Sack, A.T., Kohler, A., Bestmann, S., Linden, D.E.J., Dechent, P., Goebel, R., Baudewig, J., 2007. Imaging the brain activity changes underlying impaired visuospatial judgments: simultaneous FMRI, TMS, and behavioral studies. Cereb. Cortex N. Y. N 1991 17, 2841–2852. https://doi.org/10.1093/cercor/bhm013

Schwarzkopf, D.S., Silvanto, J., Rees, G., 2011. Stochastic Resonance Effects Reveal the Neural Mechanisms of Transcranial Magnetic Stimulation. J. Neurosci. 31, 3143–3147. https://doi.org/10.1523/JNEUROSCI.4863-10.2011

Sclar, G., Maunsell, J.H., Lennie, P., 1990. Coding of image contrast in central visual pathways of the macaque monkey. Vision Res. 30, 1–10. https://doi.org/10.1016/0042-6989(90)90123-3

Silvanto, J., Muggleton, N.G., 2008. New light through old windows: moving beyond the "virtual lesion" approach to transcranial magnetic stimulation. NeuroImage 39, 549–552. https://doi.org/10.1016/j.neuroimage.2007.09.008

Simoncelli, E.P., Heeger, D.J., 1998. A model of neuronal responses in visual area MT. Vision Res. 38, 743–761. https://doi.org/10.1016/s0042-6989(97)00183-1

Solomon-Harris, L.M., Rafique, S.A., Steeves, J.K.E., 2016. Consecutive TMS-fMRI reveals remote effects of neural noise to the "occipital face area." Brain Res. 1650, 134–141. https://doi.org/10.1016/j.brainres.2016.08.043

Tadin, D., Silvanto, J., Pascual-Leone, A., Battelli, L., 2011. Improved motion perception and impaired spatial suppression following disruption of cortical area MT/V5. J. Neurosci. Off. J. Soc. Neurosci. 31, 1279–1283. https://doi.org/10.1523/JNEUROSCI.4121-10.2011

Telesford, Q.K., Simpson, S.L., Burdette, J.H., Hayasaka, S., Laurienti, P.J., 2011. The Brain as a Complex System: Using Network Science as a Tool for Understanding the Brain. Brain Connect. 1, 295–308. https://doi.org/10.1089/brain.2011.0055

Tik, M., Woletz, M., Lara, L.N. de, Sladky, R., Hoffmann, A., Hummer, A., Windischberger, C., 2017. Mapping TMS local and remote immediate effects by concurrent TMS/fMRI using a dedicated high-sensitivity coil array. Brain Stimul. Basic Transl. Clin. Res. Neuromodulation 10, 489–491. https://doi.org/10.1016/j.brs.2017.01.432

Tu, W., Ma, Z., Zhang, N., 2021. Brain network reorganization after targeted attack at a hub region. NeuroImage 237, 118219. https://doi.org/10.1016/j.neuroimage.2021.118219

Tzourio-Mazoyer, N., Landeau, B., Papathanassiou, D., Crivello, F., Etard, O., Delcroix, N., Mazoyer, B., Joliot, M., 2002. Automated anatomical labeling of activations in SPM using a macroscopic anatomical parcellation of the MNI MRI single-subject brain. NeuroImage 15, 273–289. https://doi.org/10.1006/nimg.2001.0978

Vink, J.J.T., Mandija, S., Petrov, P.I., van den Berg, C.A.T., Sommer, I.E.C., Neggers, S.F.W., 2018. A novel concurrent TMS-fMRI method to reveal propagation patterns of prefrontal magnetic brain stimulation. Hum. Brain Mapp. 39, 4580–4592. https://doi.org/10.1002/hbm.24307

Wahlbom, A., Enander, J.M.D., Bengtsson, F., Jörntell, H., 2019. Focal neocortical lesions impair distant neuronal information processing. J. Physiol. 597, 4357–4371. https://doi.org/10.1113/JP277717

Wang, J., Wang, X., Xia, M., Liao, X., Evans, A., He, Y., 2015. Corrigendum: GRETNA: a graph theoretical network analysis toolbox for imaging connectomics. Front. Hum. Neurosci. 9.

Wu, Y., Hengen, K.B., Turrigiano, G.G., Gjorgjieva, J., 2019. Homeostatic mechanisms regulate distinct aspects of cortical circuit dynamics. bioRxiv 790410. https://doi.org/10.1101/790410

Zhang, R., Tadin, D., 2019. Disentangling locus of perceptual learning in the visual hierarchy of motion processing. Sci. Rep. 9. https://doi.org/10.1038/s41598-018-37892-x

Zhao, X., Tian, L., Yan, J., Yue, W., Yan, H., Zhang, D., 2017. Abnormal Rich-Club Organization Associated with Compromised Cognitive Function in Patients with Schizophrenia and Their Unaffected Parents. Neurosci. Bull. 33, 445–454. https://doi.org/10.1007/s12264-017-0151-0

970 **Supplementary online Materials**

971 *1.* **Motion processing localizer**: A standard h*MT+/V5* localizer task was acquired during
972 the first fMRI session and used to accurately and individually target the h*MT+/V5* area.
973 The screen displayed radially moving dots alternating with stationary dots (see e.g., [81]). A
974 block design alternated six 15 s blocks of radial motion with six blocks featuring
975 stationary white dots in a circular region on a black background. This region subtended
976 25° visual angle, with 0.5 dots per square degree. Each dot was 0.36° diameter. In the
977 motion condition the dots repeatedly moved radially inward for 2.5 s and outward for
978 2.5 s, with 100% coherence, at 20°/s measured at 15° from the center. Participants were
979 passively looking at the screen and were asked to focus on a fixation point located in the
980 middle of the screen. The motion processing localizer was acquired using a GE-EPI
981 sequence with 56 axial slices, slice thickness = 2.2 mm, in-plane resolution = 2.2 mm, TR
982 = 2000 ms, TE = 30 ms, FOV = 242 mm, flip angle = 60°, GRAPPA = 2, Multiband Factor
983 (MB) = 2.

984 **2. Additional MRI sequences for coregistration of TMS-fMRI data**

985 Functional and structural MR data, respectively acquired with the TMS-MRI coils and the
986 64-channel head coil, were found difficult to co-register due to different coil coverage,
987 sensitivity and contrast. Therefore, two additional rapid high signal-to-noise, balanced,
988 steady-state free precession (SSFP) sequences [82] (96 axial slices, slice thickness = 2 mm,
989 (gap 0.4 mm), in-plane resolution = 2 mm, TR = 5.24 ms, FOV = 256 mm, flip angle = 28°)
990 were acquired with both the TMS-MRI coils and the body coil integrated into the
991 scanner bore in order to resolve based on the same SSFP contrast the coil coverage
992 mismatch within the registration processing pipeline.

993

994 **Supplementary Figure S1 (Motion direction discrimination with late TMS onsets)**

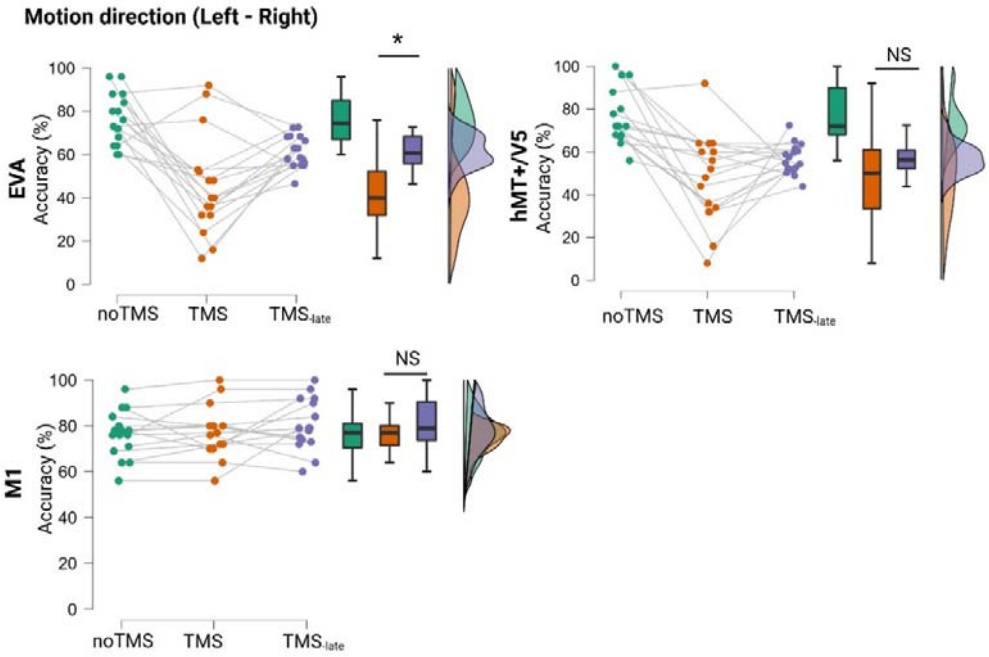

995

996 ***Figure S1:*** *Individual, group average and distribution of motion*
997 *direction discrimination without TMS, with TMS and* TMS_{-late} *for*
998 $TMS_{(EVA)}$ *(top left),* $TMS_{(hMT+/V5)}$ *(top right) and* $TMS_{(M1)}$ *(bottom row).*

999

1000

1001 **Supplementary Figure S2 (Task EVA)**

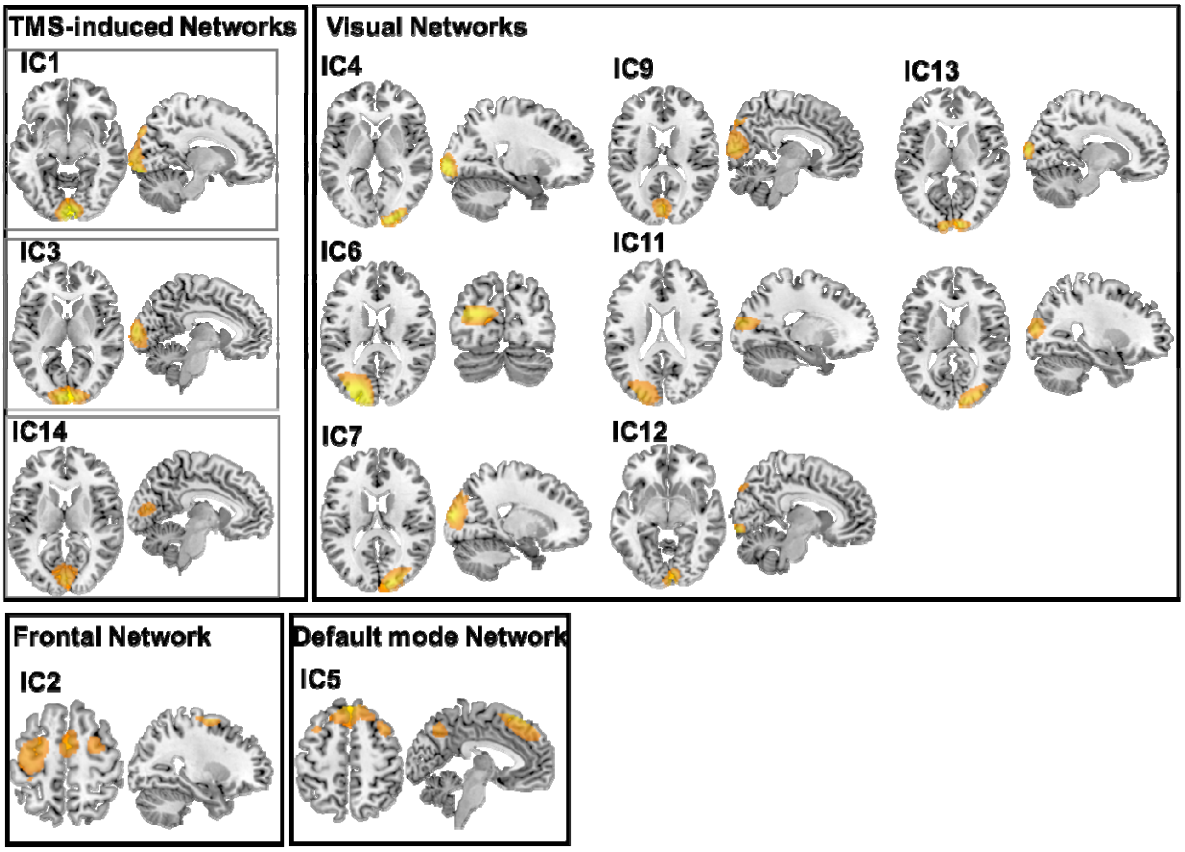

1002

1003

1004 ***Figure S2**: Independent component analysis (ICA) results of TMS$_{(EVA)}$ at rest. Spatial*
1005 *distribution of 13 networks, grouped into functional groups. See Supplementary*
1006 *Table S5 for the Montreal Neurological Institute (MNI) coordinates;*

1007

1008

1009 **Supplementary Figure S3 (Task hMT+/MT)**

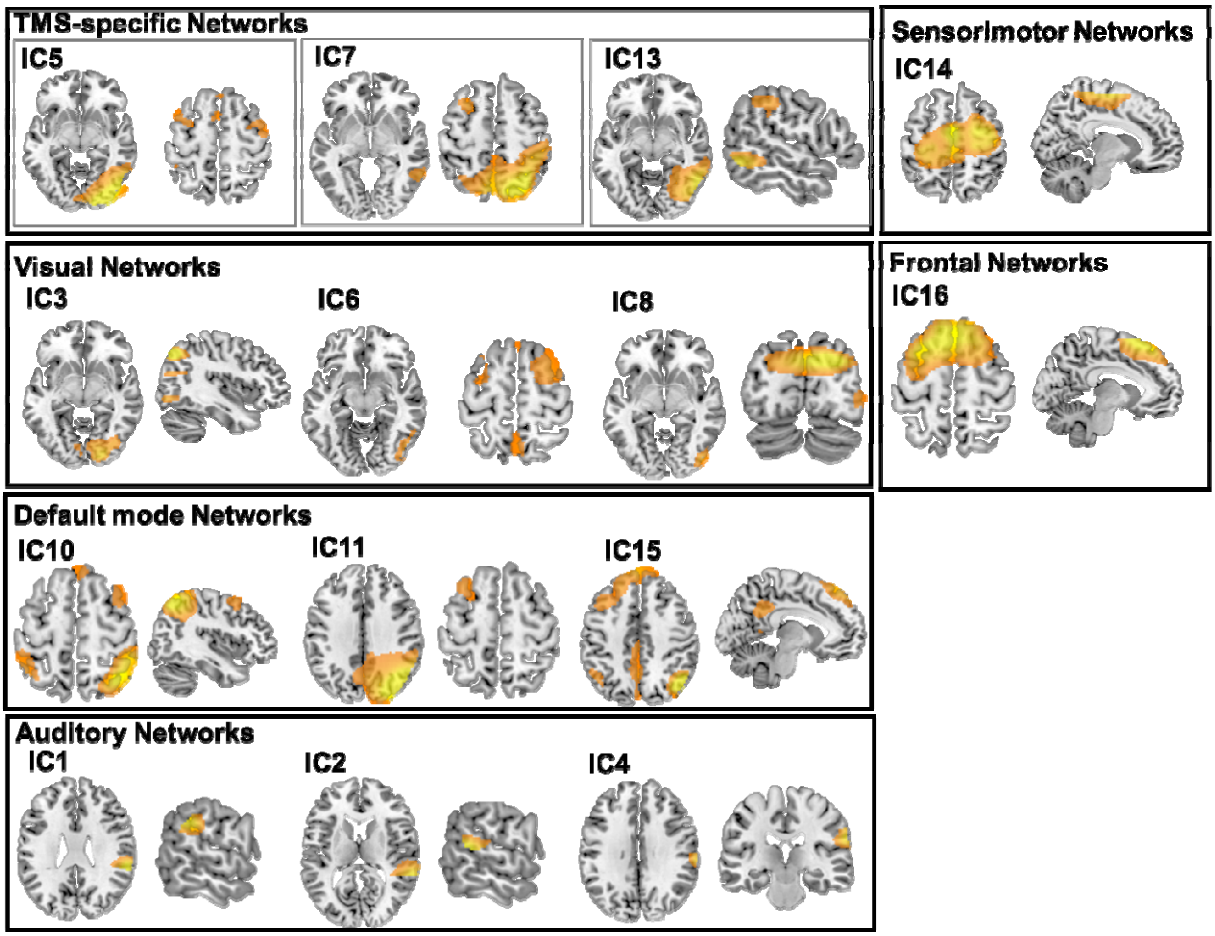

1010

1011 ***Figure S3**: Independent component analysis (ICA) results of the motion*
1012 *discrimination task with $TMS_{(EVA)}$. Spatial distribution of 13 networks, grouped into*
1013 *functional groups. See Supplementary Table S6 for the Montreal Neurological*
1014 *Institute (MNI) coordinates;*

1015

1016 **Supplementary Table S1** (GLM analysis Rest EVA)

Brain region	Cluster extent	Z score	Peak MNI coordinate		
			x	y	z
noTMS>TMS					
EVA (right hem.)	516	4.43	6	-80	15
hMT+/V5 (right hem.)	419	3.31	51	-52	10
TMS>noTMS					
SMA	219	4.48	1	2	61
FEF	384	3.91	23	8	61

1017 *Bilat.: bilateral; hem.: hemisphere; FEF: Frontal Eye Field; EVA: early visual areas; hMT+/V5:*
1018 *motion-sensitive medio-temporal visual area; SMA: supplementary motor area.*

1019

1020

1021 **Supplementary Table S2** (GLM analysis Rest hMT+/V5)

Brain region	Cluster extent	Z score	Peak MNI coordinate		
			x	y	z
noTMS>TMS					
hMT+/V5 (right hem.)	609	4.62	39	-70	-5
EVA (right hem.)	213	3.47	6	-64	-7
FEF (right hem.)	205	4.05	12	2	50

1022 *Hem.: hemisphere; FEF: Frontal Eye Field; EVA: early visual areas; hMT+/V5: motion-sensitive*
1023 *medio-temporal visual area.*

1024

1025

1026 **Supplementary Table S3** (GLM analysis Task EVA on correct moving trials)

Brain region	Cluster extent	Z score	Peak MNI coordinate		
			x	y	z
TMS>noTMS					
EVA (bilat.)	502	3.34	-2	-88	20
SMA (bilat.)	1843	3.21	2	-11	60

1027 *Bilat.: bilateral; EVA: primary visual areas; SMA: supplementary motor area;*

1028

1029 **Supplementary Table S4** (GLM analysis Task hMT+/V5 on correct moving trials)

Brain region	Cluster extent	Z score	Peak MNI coordinate		
			x	y	z
noTMS>TMS					
hMT+/V5 (Right hem.)	462	4.73	37	-61	-5
EVA	351		8	-66	-2

1030 *Hem.: hemisphere; EVA: early visual areas; hMT+/V5: motion sensitive medio-temporal visual*
1031 *area.*

1032

1033

1034 **Supplementary Table S5** (MNI coordinates of the 13 IC networks Task EVA)

Component	Cluster region	Cluster extent	Peak MNI coordinate		
			x	y	z
TMS-specific Networks					
IC1*	EVA (Bilat.)	1843	21	-93	-6
IC3*	EVA (Bilat.)	1557	-5	-85	2
IC14*	EVA (Bilat.)	1243	-1	-81	8
Visual Networks					
IC4	EVA (Right hem.)	763	28	-89	5
IC6	EVA (Left hem.)	587	-14	-93	18
IC7	EVA (Right hem.)	634	30	-93	-5
IC9	EVA (Bilat.)	1476	3	-97	9
IC11	EVA (Left hem.)	423	-24	-86	18
IC12	EVA (Bilat.)	764	5	-88	-8
IC13	EVA (Bilat.)	984	-7	-92	16
IC15	EVA (Right hem.)	478	27	-89	17
Frontal Network					
IC2	FEF (Right hem.)	642	28	-2	52
	FEF (Left hem.)	897	-31	-1	51
	SMA (Bilat.)	598	8	-5	66
Default Mode Networks					
IC5	Pre Frontal	2534	6	43	45
	Pre Cuneus	1243	2	-66	43

1035 *Bilat.: bilateral; hem.: hemisphere; FEF: Frontal Eye Field; EVA: early visual areas; SMA:*
1036 *supplementary motor area;* Networks significantly modulated by TMS*

1037

1038 **Supplementary Table S6** (MNI coordinates of the 14 IC networks Task hMT+/V5)

Component	Cluster region	Cluster extent	Peak MNI coordinate		
			x	y	z
TMS specific Networks					
IC5*	hMT+/V5 (Right hem.)	1343	58	-48	1
	FEF (Right hem.)	187	54	-18	45
	FEF (Left hem.)	218	-32	-24	58
	PreSMA (bilat.)	138	4	15	61
IC7*	hMT+/V5 (Right hem.)	348	43	-73	16
	PPC (bilat.)	3577	26	-59	56
	PreFrontal (Left hem.)	298	9	-21	57
	PPC (bilat.)	2232	30	-69	60
IC13*	V5 (Right hem.)	1687	9	3	45
	PPC (Right hem.)	587	39	-21	20
Visual Network					
IC3	EVA (Right hem.)	4420	-3	-78	2
	PPC (Right hem.)	221	34	-45	61
IC6	hMT+/V5 (Right hem.)	122	51	-48	5
	PreCuneus (bilat.)	283	-3	-19	12
	FEF (Right hem.)	934	27	12	653
	FEF (Left hem.)	189	-31	17	65
IC8	hMT+/V5 (Right hem.)	132	56	-58	4
Sensorimotor Network					
IC14	SM1 (bilat.)	4286	25	-20	63
Frontal Network					
IC16	Frontal lobe (bilat.)	3984	-4	29	55
Default Mode Networks					
IC10	FEF (Right hem.)	234	38	20	59
	PPC (Right hem.)	1384	40	-50	59
	PPC (Left hem.)	984	45	-46	54
	mPFC (bilat.)	346	3	51	42
IC11	PPC (Right hem.)	1583	40	-50	59
	PFC (Left hem.)	219	46	28	44
IC15	PPC (Right hem.)	1032	50	-59	44
	PPC (Left hem.)	783	-43	-53	44
	PCC	2984	1	-54	42
	PFC	2439	2	36	46
Auditory Networks					

IC1	STG	274	57	-52	6
IC2	TPJ	355	54	-57	21
IC4	STG	254	60	-43	7

Bilat.: bilateral; hem.: hemisphere; hMT+/V5: motion-sensitive medio-temporal visual area; FEF: Frontal Eye Field; EVA: early visual areas; mPFC: medial prefrontal cortex; PCC: posterior cingulate cortex; ACC: anterior cingulate cortex; SMA: supplementary motor area; LGN: lateral geniculate nucleus; S1: preimary somatosensory cortex.

1046 **Supplementary Table S7** (paired t-tests for Sigma compared between $TMS_{(EVA)}$ and
1047 $TMS_{(hMT+/V5)}$ networks)

Sparcity thresholds	t	df	p
0.05	0.084	14	0.23
0.1	0.121	14	0.24
0.15	0.31	14	0.45
0.2	0.52	14	0.26
0.25	0.84	14	0.16
0.3*	2.01	14	0.03
0.35	1.89	14	0.06
0.4*	2.01	14	0.03
0.45*	2.02	14	0.04
0.5	1.45	14	0.17

1048 **: Significant difference in smallworldness (Sigma) between EVA and hMT+/V5 networks.*

1049

1050

Supplementary Table S8 (paired t-tests for Lambda compared between $TMS_{(EVA)}$ and $TMS_{(hMT+/V5)}$ networks)

Sparcity thresholds	t	df	p
0.05	0.237	14	0.82
0.1	0.175	14	0.86
0.15	0.128	14	0.9
0.2	0.26	14	0.8
0.25	0.5	14	0.62
0.3	0.713	14	0.5
0.35	0.845	14	0.42
0.4	0.946	14	0.36
0.45	1.089	14	0.2
0.5	1.089	14	0.28

1055 **Supplementary Table S9** (paired t-tests for Gamma compared between $TMS_{(EVA)}$ and
1056 $TMS_{(hMT+/V5)}$ networks)

Sparcity thresholds	t	df	p
0.05	0.452	14	0.66
0.1	-0.72	14	0.49
0.15(*)	-1.9	14	0.08
0.2*	-2.03	14	0.05
0.25*	-2.16	14	0.04
0.3	-1.45	14	0.17
0.35	-1.2	14	0.25
0.4	-0.75	14	0.47
0.45	-0.8	14	0.43
0.5	-0.77	14	0.46

1057 **: Significant difference in Path Length (Gamma) between EVA and hMT+/V5 networks.*

1058

1059

1060